This project has received funding from the European Union's Seventh Programme for research, technological development and demonstration under grant agreement No [308417]".

New Directions in Seismic Hazard Assessment through Focused Earth Observation in the Marmara Supersite

Grant Agreement Number: 308417
co-funded by the European Commission within the Seventh Framework Programme
THEME [ENV.2012.6.4-2]
[Long-term monitoring experiment in geologically active regions of Europe prone to natural hazards: the Supersite concept]

D5.3

Performance assessment of finite-fault inversion codes in the Marmara configuration

Project Start Date	1 November 2012
Project Duration	36 months
Project Coordinator /Organization	Nurcan Meral Özel / KOERI
Work Package Number	WP5
Deliverable Name/ Number	Performance assessment of finite-fault inversion codes in the Marmara configuration/D5.3
Due Date Of Deliverable	30 April 2015
Actual Submission Date	11 May 2015
Organization/Author (s)	INGV, GFZ, BRGM/ Cirella A., Piatanesi A.,Diao F., Wang R., Aochi H.

Dissemination Level		
PU	Public	
PP	Restricted to other programme participants (including the Commission)	
RE	Restricted to a group specified by the consortium (including the Commission)	
CO	Confidential, only for members of the consortium (including the Commission)	

TABLE OF CONTENTS

1. Introduction

Two different finite-fault techniques have been proposed and tested, from BRGM, INGV and GFZ researchers' team. In order to assess the performances of the inversion codes, in term of accuracy of the solution for the Marmara Sea tectonic setting and observational network; BRGM' team formulated a checker-board test and produced two synthetic datasets, by taking into account a planned stations configuration (strong motion, cGPS, GPS, BB), in the Marmara region and by assuming a given velocity 1D profile and a 3D crustal structure. INGV and GFZ teams used this datasets to perform kinematic inversion of the slip distribution on the corresponding finite-fault. These tests have the principal aim to assess the performance of the inversion codes in the Marmara configuration.

2. Checker board test

2.1 Description of checker board test

The area of interest is prepared for a dimension of 200 km (East-West) x 120 km (North-South) around the Sea of Marmara, including the region of Istanbul (WP5.3). The wave propagation in the elastic medium is calculated using a 3D finite difference method (Aochi et al., 2013). Any finite source scenario can be included anywhere in the model. For the verification test, we prepare a kinematic source model whose slip distribution is checker-board-like feature on a fault plane. The given parameters are in the following (also informed to the participants). In particular, the distribution of four asperities and rupture time are shown in Figure 1.

Parameter	**Value**
Hypocenter	28.3965°E, 40.8549°N, 7 km depth
Fault Plane	96 km (length) x 24 km (width)
Mechanism	Strike N86°E, Dip 90°, Rake 180°
Eastern end of fault plane	28.870°E, 40.880°N
Top of fault plane	0.5 km
Asperity size	16 km x 8 km
Slip amount	1 m on asperities/ 0 m elsewhere
Rupture velocity	2.1 km/s
Rise time (triangle function)	2.5 s

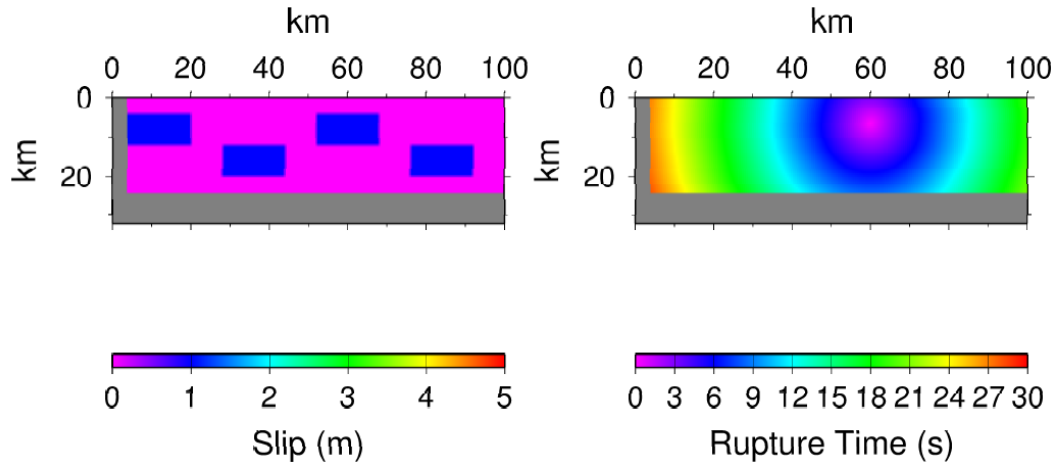

Figure 1. The given slip distribution (left) and rupture time (right) on a fault plane.

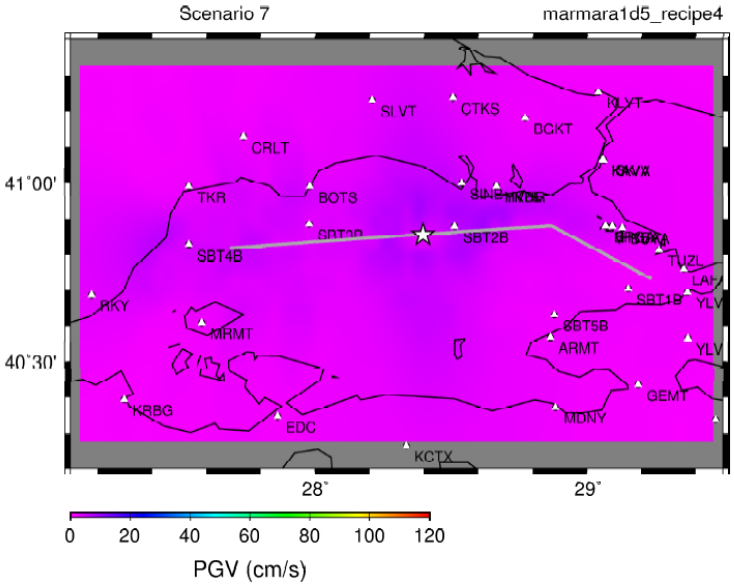

Figure2. Illustration of the hypocenter, the fault position (strike N86°E) and the 47 receiver positions. The eastern part of the fault (running to SE) is not used in this inversion test. The color presents a Peak Ground Velocity (PGV) from the simulation using a 3D structure.

For the purpose of the inversion, the synthetic ground motions are calculated and saved for the 47 receivers according to the real locations from the observation network of the region (Figure 2). The seismograms (velocity in m/s) are not filtered, with a time step of 0.01 seconds for a duration of 120 seconds for the three components. These data can be downloaded from http://aochi.hideo.perso.neuf.fr/marmara/ (scenario 7). The ground motions are calculated in the two structure models:

1. 1D layered structure,
2. 3D structure.

The used 1D layered structure is the following:

Top of layer (km)	Vp (m/s)	Vs (m/s)	Density (kg/m3)	Q*
0	2250	1100	2150	300
-1	5700	3200	2700	300
-6	6100	3600	2750	300
-20	6800	3850	2800	300
-33	8000	4550	2850	300

* Qualitiy factor Q is included as a dumping factor in the finite difference formulation.

The 3D structure (Figure3) was prepared in WP5.3, by a combination of 3D tomography result around the Sea of Marmara (Bayrakci et al., 2013) and a regional 1D model (Karabulut, personal comm.). We also adjusted the bathymetry from the 30 seconds-model of GEBCO so that we introduce a layer of Sea of Marmara, letting Vp = 1500 m/s and Vs = 0 m/s (Aochi and Ulrich, ECEES, 2014; Aochi and Ulrich, BSSA, 2015).

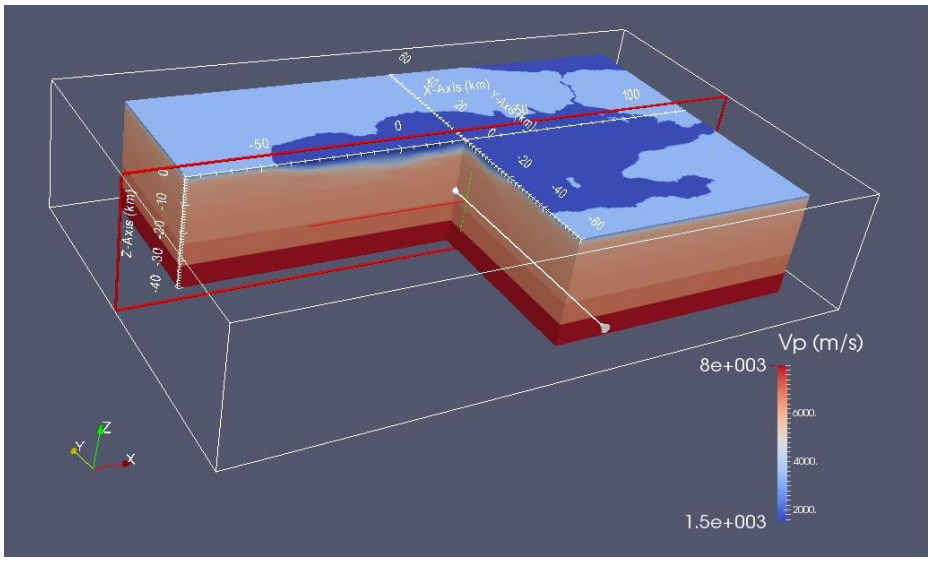

Figure3. The used 3D structure model (Vp structure).

The two cases allow each partner to check the resolution in their inversion procedure.

2.2 GFZ' TEAM RESULTS

2.2.1 Methodology

To reduce user's subjective influence on the inversion results, Zhang et al. (2014) proposed a new kinematic inversion scheme, called the iterative deconvolution and stacking (IDS) method. We use this method for all of our inversions in the Marsite Project. In the IDS method, synthetic Green's function deconvolution is applied to the waveform data to obtain apparent subfault source-time-functions from different stations. In most cases, the

deconvolution and stacking procedure needs to be applied iteratively to resolve a complex multiple rupture process. In fact, the IDS method benefits from the complementary advantages between the traditional least-squares inversion and the array back-projection techniques. The work flow that shown in Fig. 4 draw the main steps of the IDS inversion method:

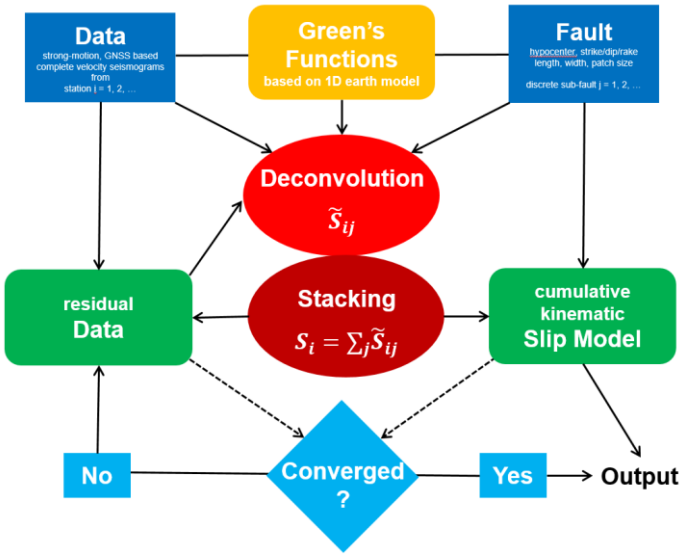

Figure4. Simple work flow of the IDS inversion method.

The IDS method aims at robust and rapid estimation of the main character of the rupture process. Because it is largely free of empirical constraints such as rupture velocity, rise time and shape of subfault source time function, the inversions by using IDS don't give a direct estimation of rupture velocity and rise time.

2.2.2 Geometrical setting- Fault parametrization - Data processing

Based on the 1D model provided by H. Aochi, a Green's function database is prepared using the code QSEIS developed by Wang (1999). The fault plane (120 km × 24 km) that constructed based on the focal mechanism (strike=86°, dip=90°) was discretized to 180 subfaults of 4 km × 4 km size, each being treated as a point source. We fixed the rake angle to be 180°. We did not constraint the rupture velocity, rise time and the shape of the rise time. Firstly we filter the original synthetic data in form of velocity seismograms first with a 3rd-order Butterworth high-pass filter of 0.02 Hz to remove the influence caused by the low-frequency numerical drift in the data, and then with a causal low-pass filter corresponding to Brunes near-field velocity spectrum;

$$L(f) = \frac{1}{(1+if/f_c)^2} \quad (1)$$

where f_c is called the corner frequency. Thus, our waveform data trend to the velocity seismograms only for $f \ll f_c$. They become proportional to the displacement seismograms when $f \sim f_c$ and to the integral of displacement seismograms when $f \gg f_c$. The advantage of using the low-pass filter defined by Eq. (1) is that no sharp high-frequency cutoff is necessary. With higher corner frequencies used, more high-frequency components will be used in our inversion. So, the frequency band used in our inversion is different with many previous studies of kinematic source inversions.

2.2.3 Results

The results by inverting different synthetic data are shown in Fig. 5, from which we found that the input four asperities are clearly identified. Based on the data processing approach used in our study, inversions were carried out by using the three different corner frequencies (0.05 Hz, 0.10 Hz and 0.20 Hz). The inverted results (Fig. 5) indicate that the input asperities can be well captured, although different corner frequencies were used for the inversions. Moreover, it is not surprising to find a better resolution by using higher corner frequencies.

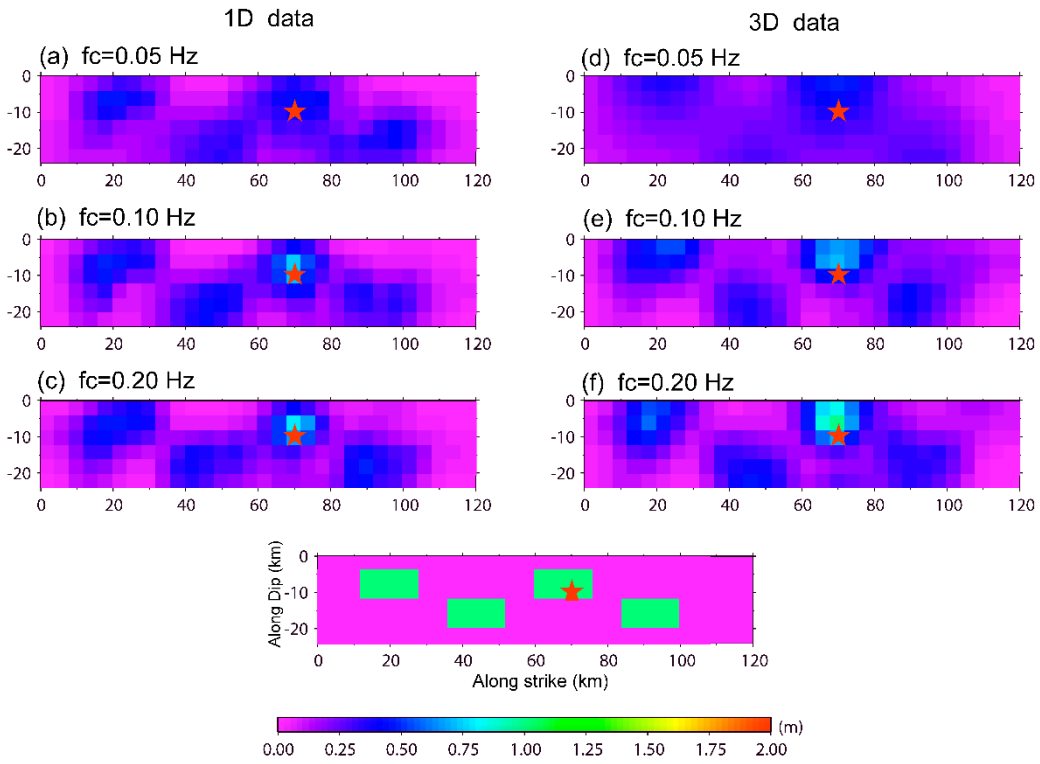

Figure 5. Rupture model inverted based on IDS method and synthetic datasets that simulated from 1D and 3D earthquake structure. (a) – (c) show rupture models inverted based on synthetic data generated from 1D earth structure, while (d) – (f) show rupture models inverted based on synthetic data generated from 3D earth structure. (g) shows the input model of the checkerboard test.

As an accurate 1D earth structure was applied, the data fit is very good for rupture models inverted by using synthetic data that generated from the same 1D earth structure (Fig. 6 – Fig. 8). However, the data fit decrease when synthetic data generated from 3D earth

structure was used (Fig. 9 – Fig. 11), which perhaps mainly induced by 3D wave propagation effect. The computation time used for inversion of the six rupture models varies between **75 second** to **200 seconds**, which increase as higher frequencies were used. All inversions were done with a PC (Intel(R) Core (TM) i7-3770 CPU @3.4G Hz, 32 GB RAM). We highlight the good efficiency of the IDS inversion, which may play an important role in earthquake rapid response.

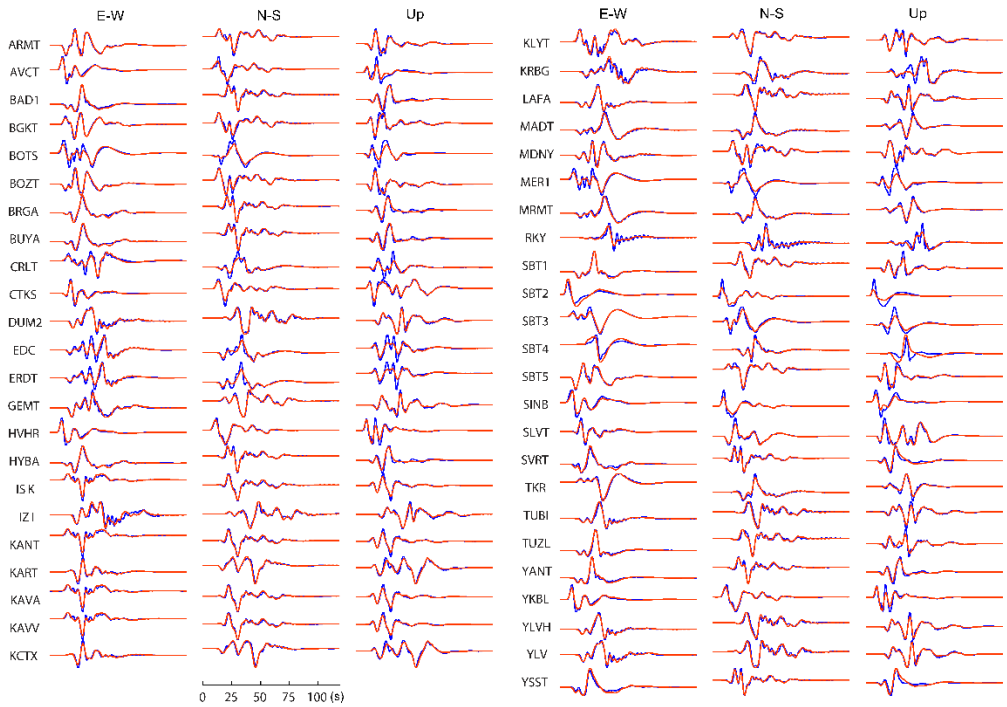

Figure 6. Waveform comparison between synthetic (blue) and inverted (red) velocity seismograms, corresponding to rupture model shown in Fig. 5(a).

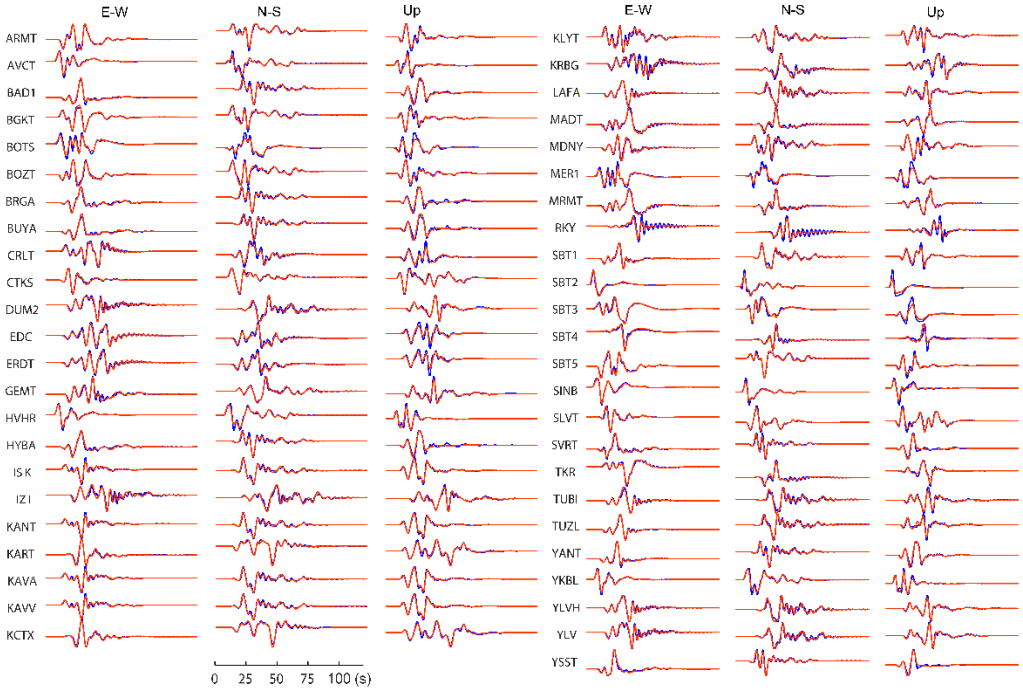

Figure 7. Waveform comparison between synthetic (blue) and inverted (red) velocity seismograms, corresponding to rupture model shown in Fig. 5(b).

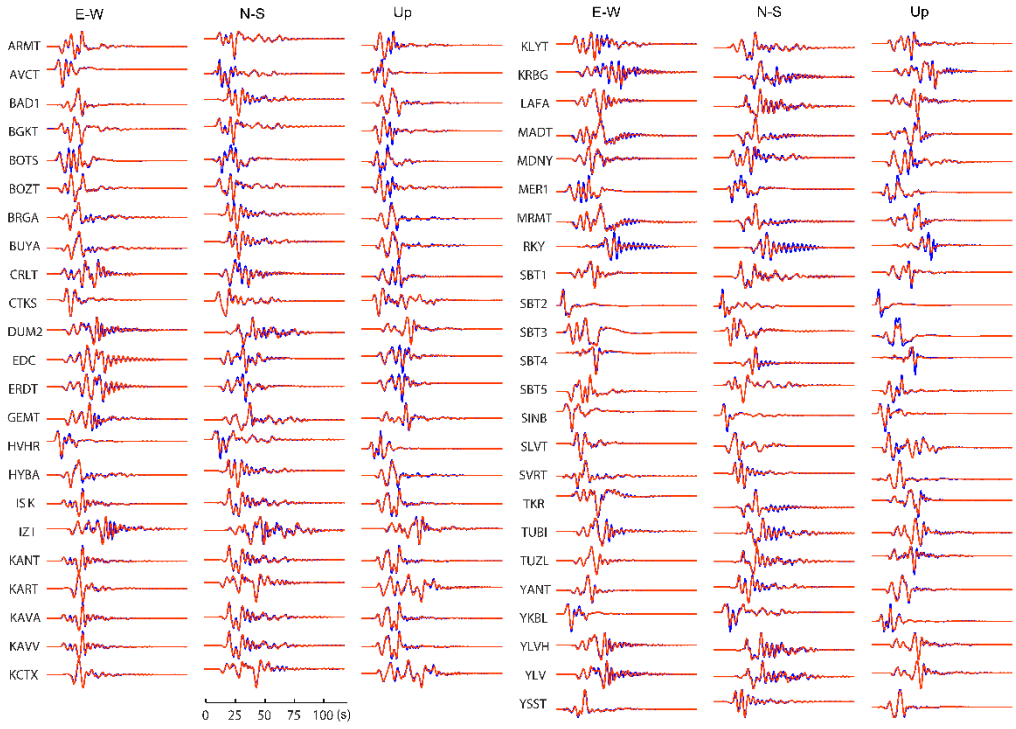

Figure 8. Waveform comparison between synthetic (blue) and inverted (red) velocity seismograms, corresponding to rupture model shown in Fig. 5(c).

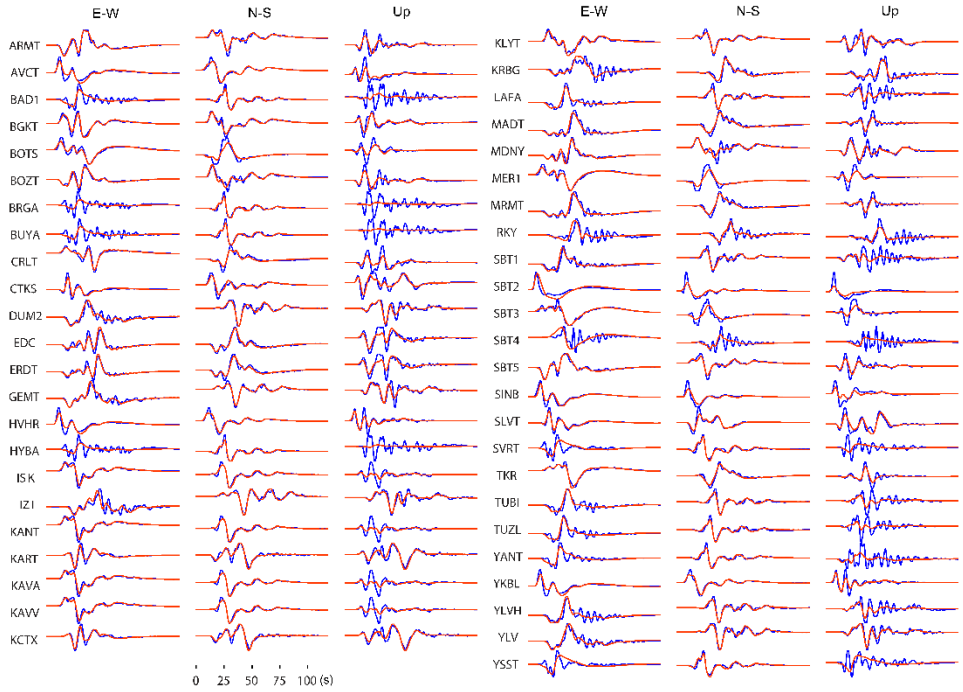

Figure 9. Waveform comparison between synthetic (blue) and inverted (red) velocity seismograms, corresponding to rupture model shown in Fig. 5(d).

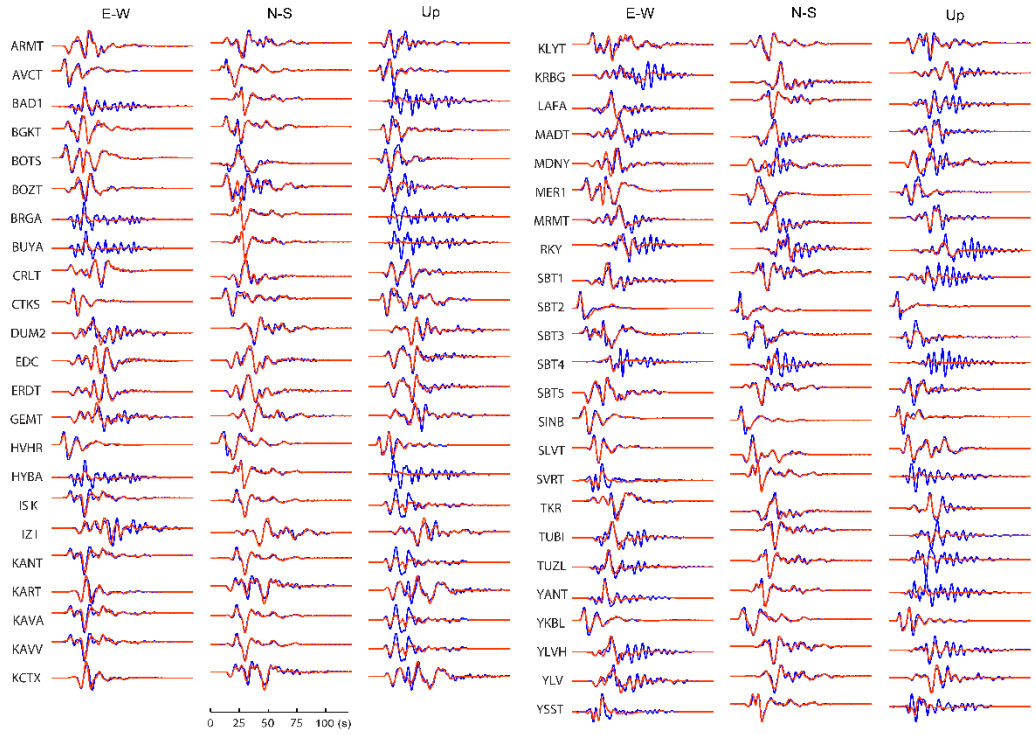

Figure 10. Waveform comparison between synthetic (blue) and inverted (red) velocity seismograms, corresponding to rupture model shown in Fig. 5(e).

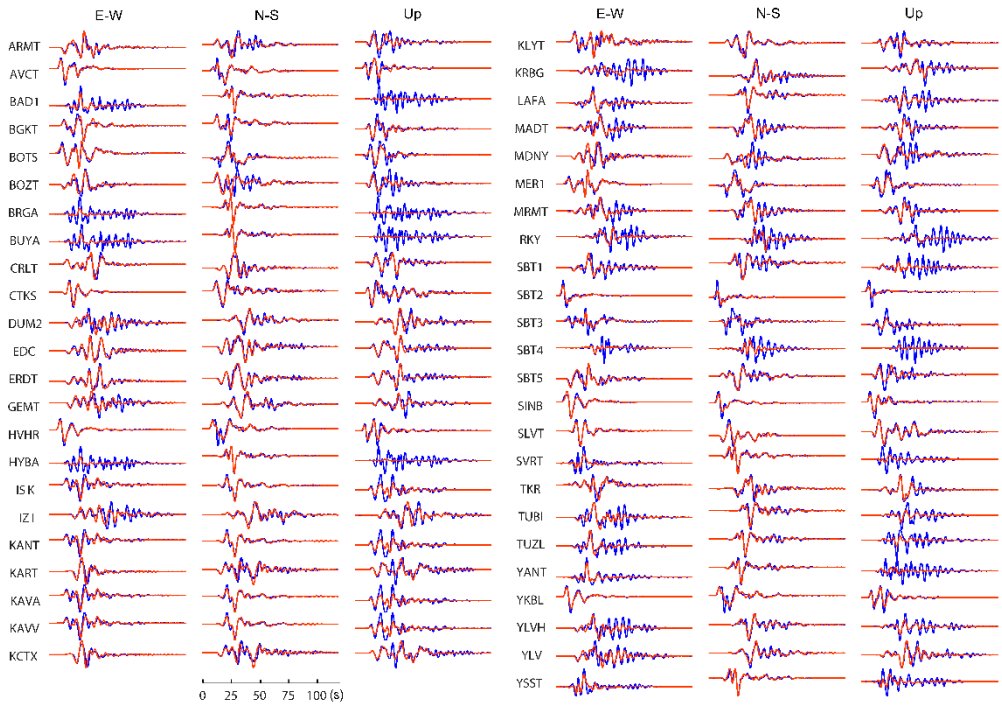

Figure 11. Waveform comparison between synthetic (blue) and inverted (red) velocity seismograms, corresponding to the rupture model shown in Fig. 5(f).

2.3 INGV' TEAM RESULTS

2.3.1 Methodology

The inversion methodology, developed at INGV, is a two-stage nonlinear technique (Piatanesi et al., 2007, Cirella et al., 2012), which involves the joint inversion of strong motion records and geodetic data. To account for rupture complexity, the model is described by four spatially variable fault parameters - peak slip velocity, slip direction, rupture time and rise time. The final slip distribution is derived by the inverted parameters. The finite fault is divided into sub-faults with model parameters assigned at the corners, whereas the parameters within each sub-fault are allowed to vary through bilinear interpolation of the nodal values. Each point on the fault can slip only once (single window approach) and the source time function can be selected among different analytical forms (box-car; cosine; regularized Yoffe function). The forward modeling is performed with a discrete wavenumber technique (Compsyn, Spudich and Xu, 2003), whose Green's functions include the complete response of the vertically varying Earth structure. The nonlinear global inversion consists of two stages. During the first stage of the inversion, a heat-bath simulated-annealing algorithm explores the model space to generate an ensemble of models that efficiently sample the good data-fitting regions. In the second stage (appraisal), the algorithm performs a statistical analysis of the model ensemble providing us the best-fitting model, the average model and the associated standard deviation, computed by weighting all models of the ensemble by the inverse of their cost function values.

2.3.2 Geometrical setting- Fault parametrization - Data processing

We used the 47 synthetic seismograms provided for Scenario7 (http://aochi.hideo.perso.neuf.fr/marmara/). Original ground velocity time histories are band-pass filtered in two different frequency ranges; between 0.01 and 0.5 Hz and between 0.01 and 0.25Hz, by using a two-pole and two-pass Butterworth filter. We invert 60 seconds of each waveform, including body and surface waves. We assumed a fault plane consistent with the hypocentre location and the focal mechanisms given for Scenario7 (strike: 86°; dip=90°; strike=180°). The fault plane is 100 km long and 24 km width, along strike and down-dip direction, respectively. We invert simultaneously for kinematic parameters at nodal points equally spaced (4.0 km) along strike and down-dip directions. During the inversion, we fix a given range of variability for each model parameter. Peak slip velocity values can range between 0 and 1.5 m/s at 0.25 m/s interval; the rise time between 1.5 and 3 sec at 0.25 sec interval. Rupture velocity is fixed to 2.1 km/s and rake angle is fixed to 180°. In this study, the adopted source time function is a modified cosine function (Ji et al. , 2002).

2.3.3 Results

We performed eight different inversions:

1. by using the dataset given for the 1D velocity model and by inverting for peak slip velocity. Rise time is fixed to 2.5 s; the inversion is performed in the frequency band 0.01-0.25Hz (results are referred as case '1DonlySlip_0.25Hz');
2. by using the dataset given for the 1D velocity model and by inverting for peak slip velocity and rise time; the inversion is performed in the frequency band 0.01-0.25Hz (results are referred as case '1DSlipRise_0.25Hz');
3. by using the dataset given for the 1D velocity model and by inverting for peak slip velocity. Rise time is fixed to 2.5 s; the inversion is performed in the frequency band 0.01-0.5Hz (results are referred as case '1DonlySlip_0.5Hz');
4. by using the dataset given for the 1D velocity model and by inverting for peak slip velocity and rise time; the inversion is performed in the frequency band 0.01-0.5Hz (results are referred as case '1DSlipRise_0.5Hz');
5. by using the dataset given for the 3D velocity model and by inverting for peak slip velocity. Rise time is fixed to 2.5 s; the inversion is performed in the frequency band 0.01-0.25Hz (results are referred as case '3DonlySlip_0.25Hz');
6. by using the dataset given for the 3D velocity model and by inverting for peak slip velocity and rise time; the inversion is performed in the frequency band 0.01-0.25Hz (results are referred as case '3DSlipRise_0.25Hz');
7. by using the dataset given for the 3D velocity model and by inverting for peak slip velocity. Rise time is fixed to 2.5 s; the inversion is performed in the frequency band 0.01-0.5Hz (results are referred as case '3DonlySlip_0.5Hz');
8. by using the dataset given for the 3D velocity model and by inverting for peak slip velocity and rise time; the inversion is performed in the frequency band 0.01-0.5Hz (results are referred as case '3DSlipRise_0.5Hz').

For each inversion we show (see Figures 12-14-16-18-20-22-24-26) the retrieved rupture model, given in terms of rise time and slip distribution on the fault plane (bottom and upper panel, respectively) and the corresponding comparison between synthetic (blue lines) and inverted (red lines) velocity time histories (see Figures 13-15-17-19-21-23-25-27).

Case: 1DonlySlip_0.25Hz

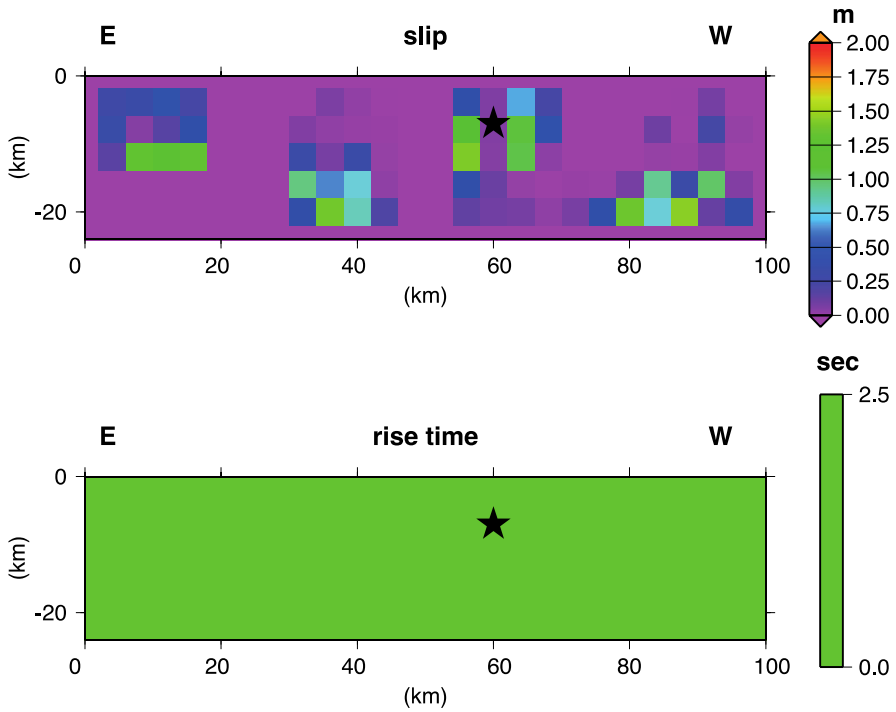

Figure12. Retrieved rupture model, in terms of slip and rise time distribution (upper and bottom panel, respectively), obtained by inverting for peak slip velocity, the 1D dataset in the frequency band 0.01-0.25Hz.

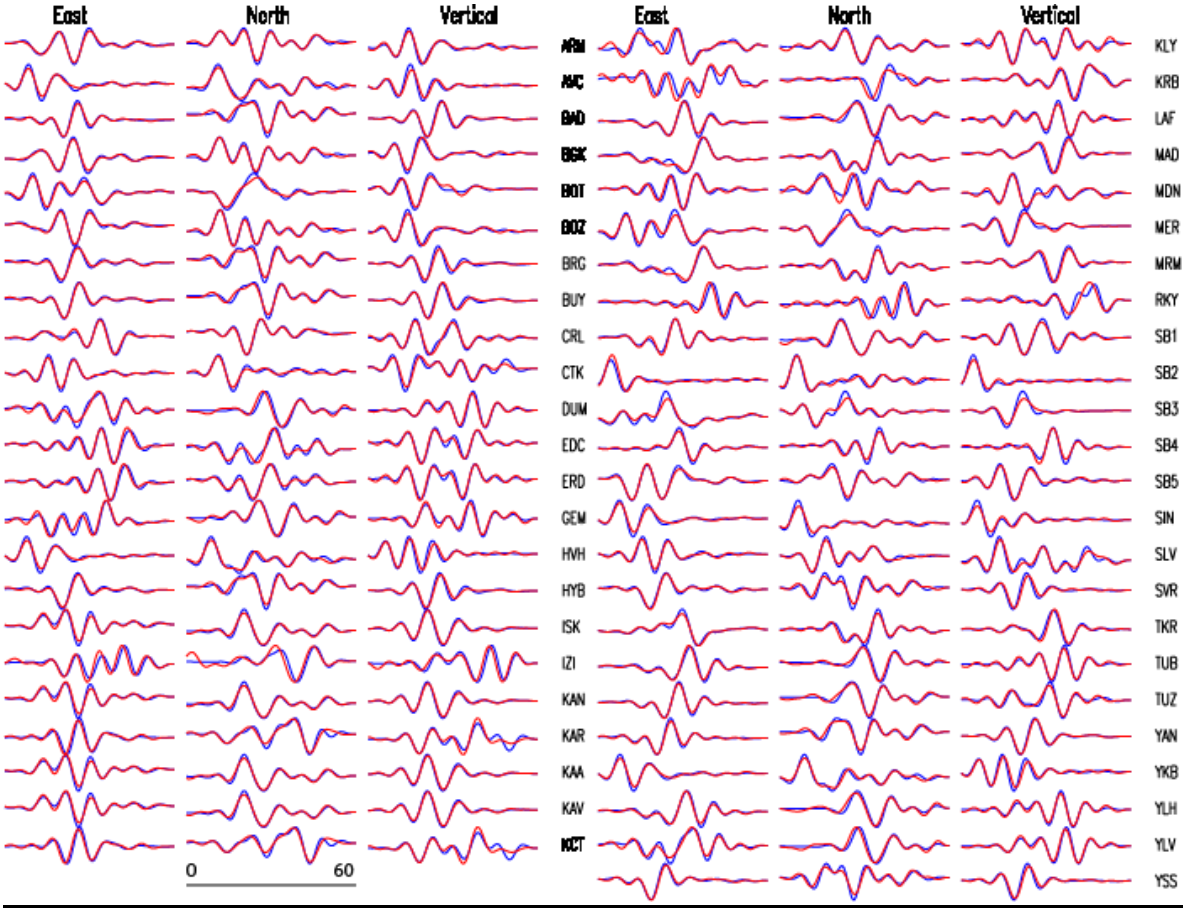

Figure13. Misfit between synthetic ground velocities (blue lines) with those computed from the inverted rupture model displayed in Figure12 (red lines).

Case: 1DSlipRise_0.25Hz

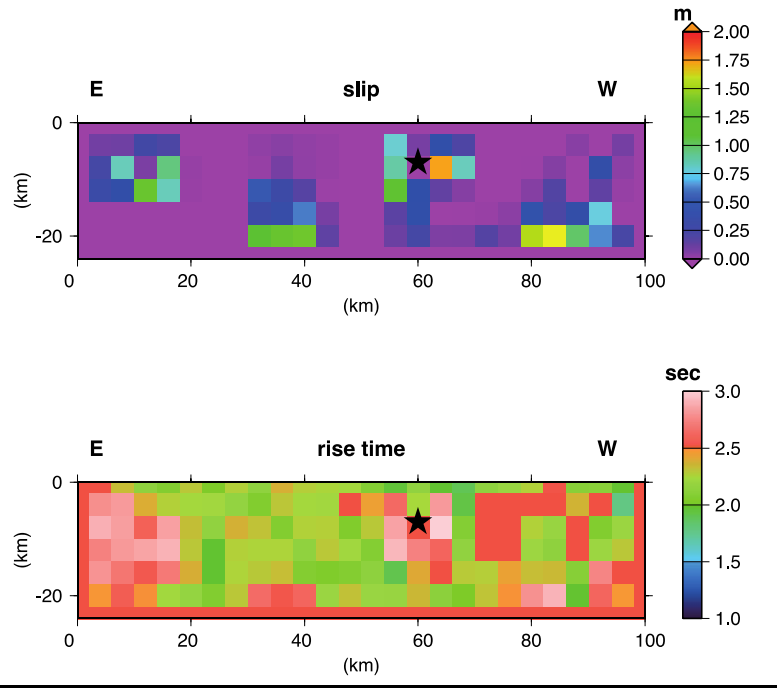

Figure14. Retrieved rupture model, in terms of slip and rise time distribution (upper and bottom panel, respectively), obtained by inverting for peak slip velocity and rise time, the 1D dataset in the frequency band 0.01-0.25Hz.

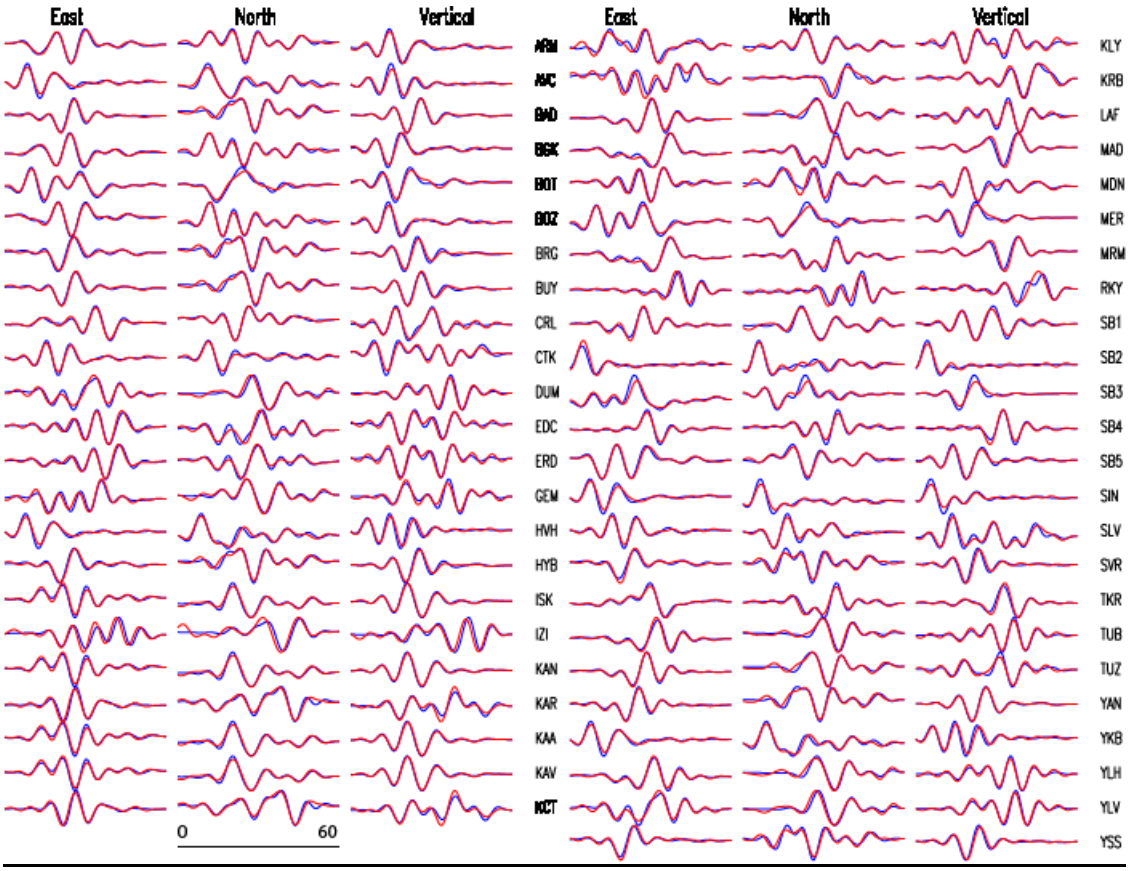

Figure15. Misfit between synthetic ground velocities (blue lines) with those computed from the inverted rupture model displayed in Figure14 (red lines).

Case: 1DonlySlip_0.5Hz

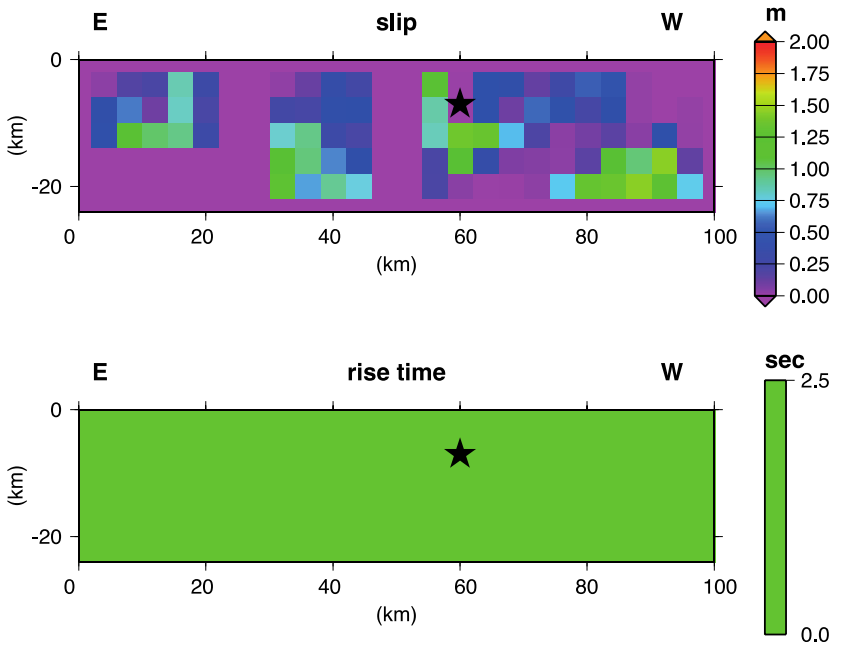

Figure16. Retrieved rupture model, in terms of slip and rise time distribution (upper and bottom panel, respectively), obtained by inverting for peak slip velocity, the 1D dataset in the frequency band 0.01-0.5Hz.

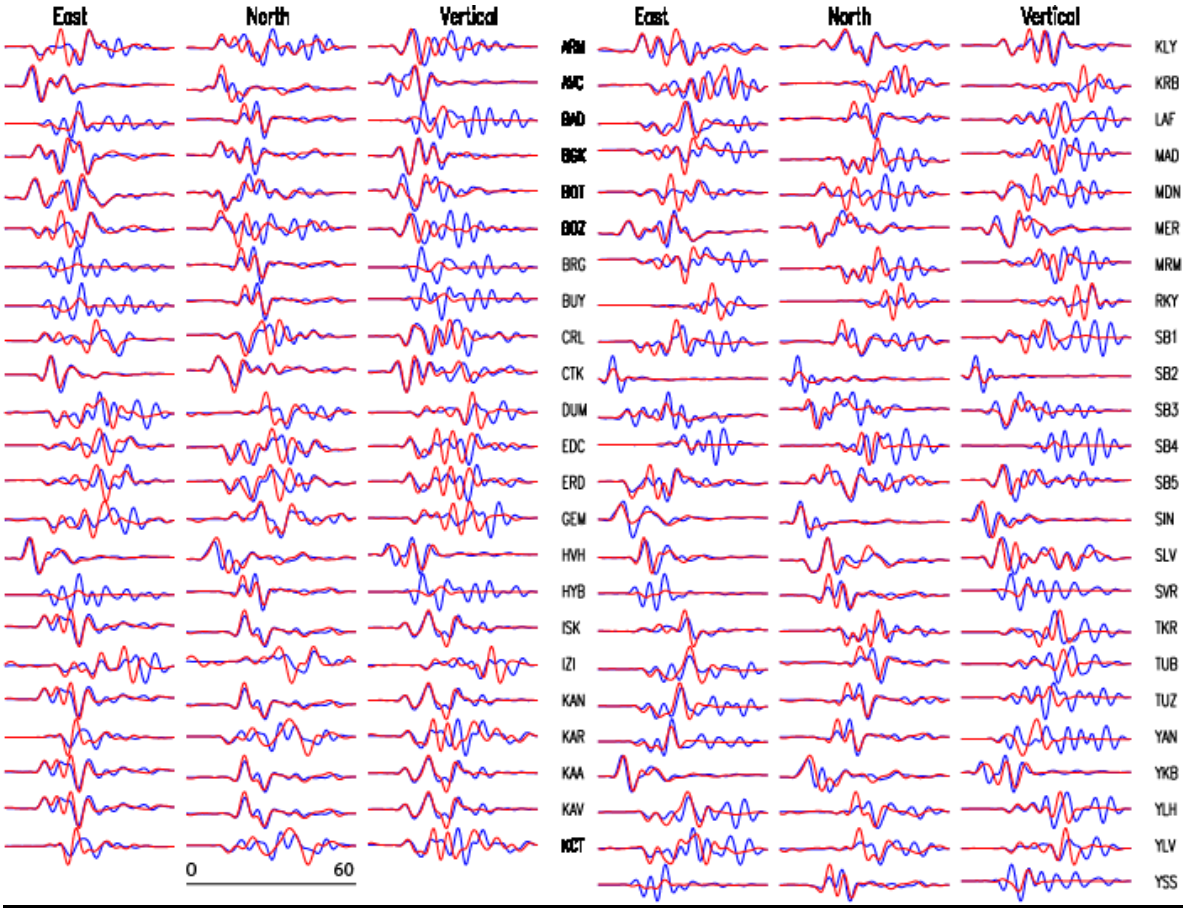

Figure17. Misfit between synthetic ground velocities (blue lines) with those computed from the inverted rupture model displayed in Figure16 (red lines).

Case: 1DSlipRise_0.5Hz

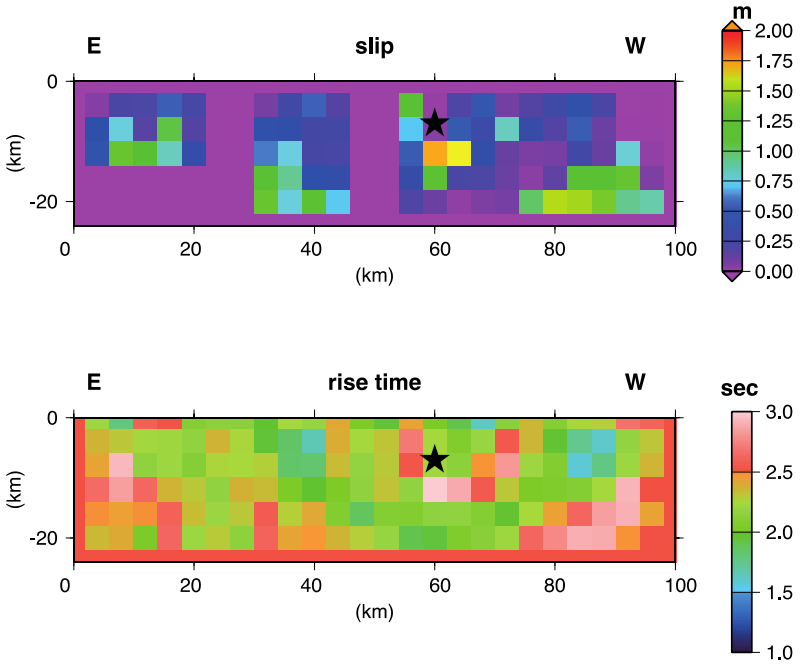

Figure18. Retrieved rupture model, in terms of slip and rise time distribution (upper and bottom panel, respectively), obtained by inverting for peak slip velocity and rise time, the 1D dataset in the frequency band 0.01-0.5Hz.

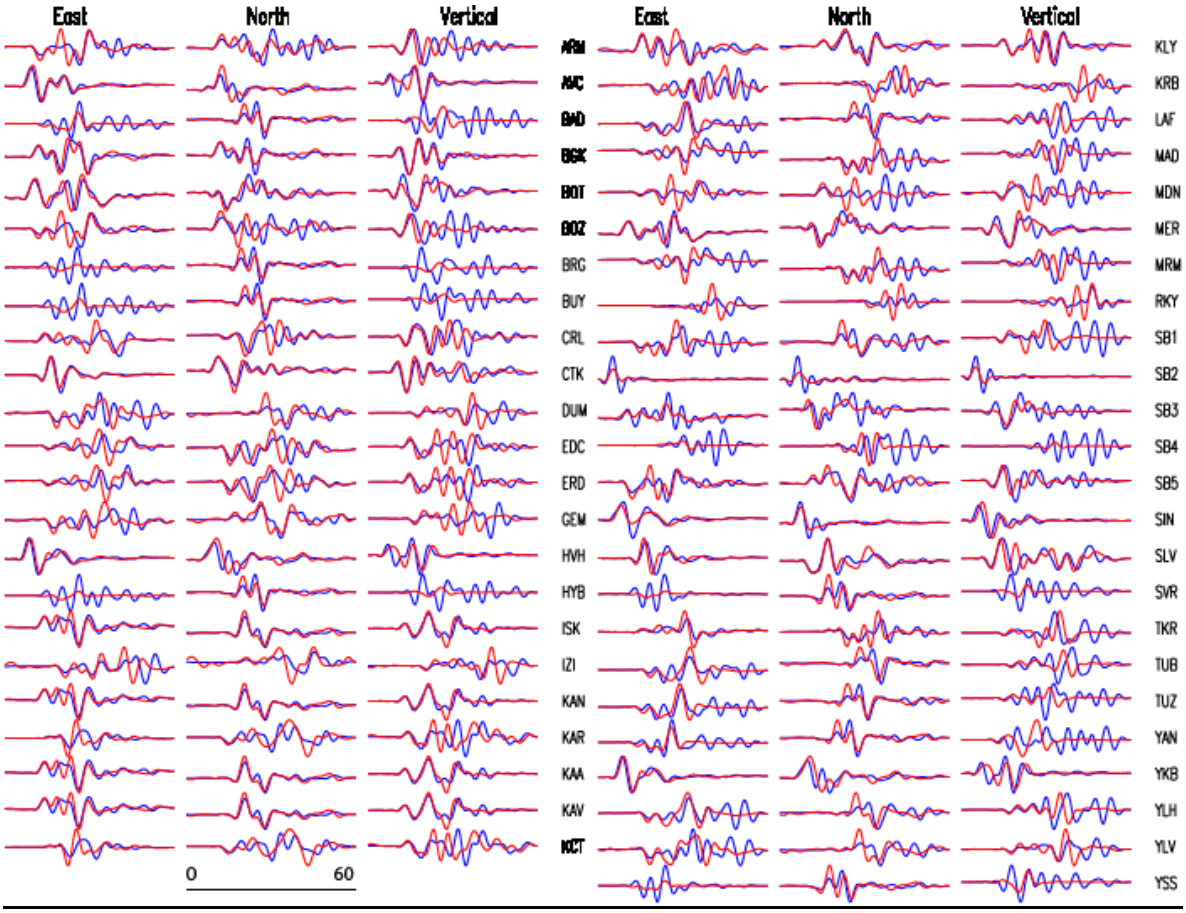

Figure19. Misfit between synthetic ground velocities (blue lines) with those computed from the inverted rupture model displayed in Figure18 (red lines).

Case: 3DonlySlip_0.25Hz

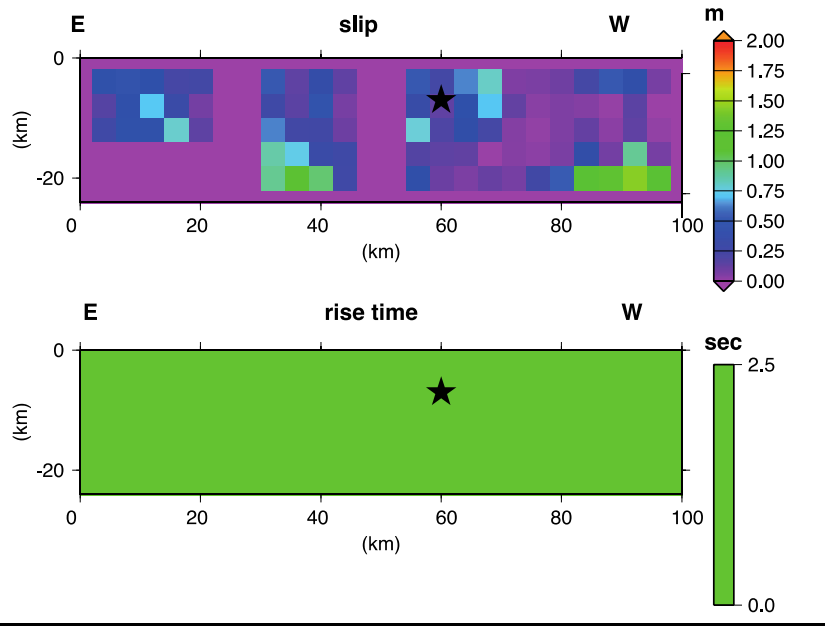

Figure20. Retrieved rupture model, in terms of slip and rise time distribution (upper and bottom panel, respectively), obtained by inverting for peak slip velocity, the 3D dataset in the frequency band 0.01-0.25Hz.

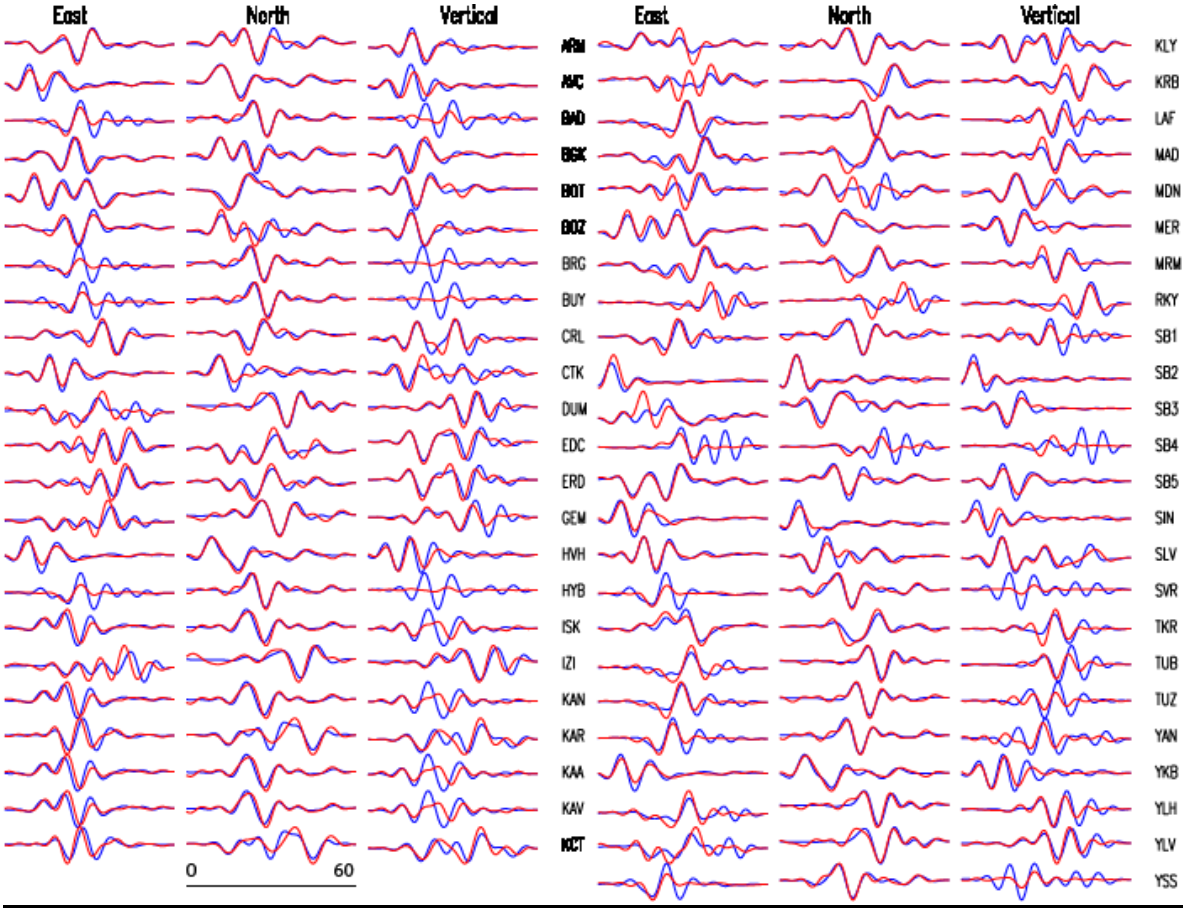

Figure21. Misfit between synthetic ground velocities (blue lines) with those computed from the inverted rupture model displayed in Figure20 (red lines).

Case: 3DSlipRise_0.25Hz

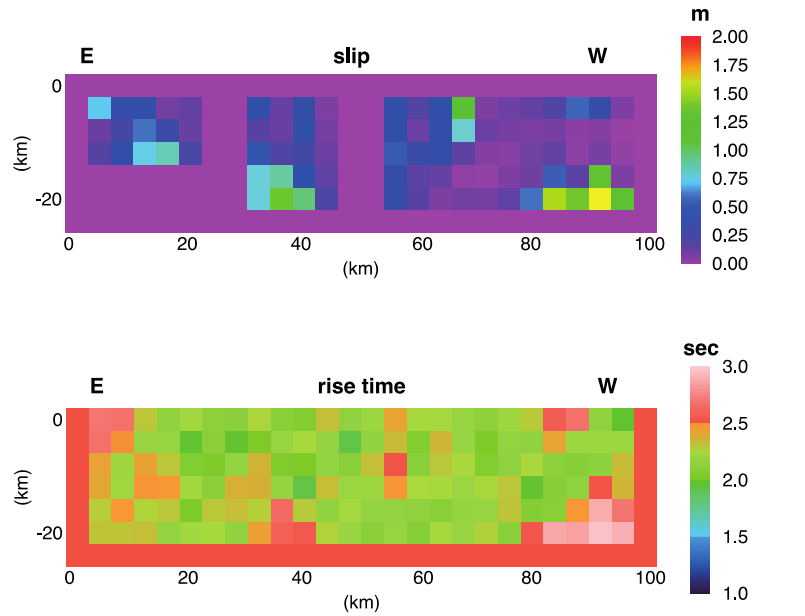

Figure22. Retrieved rupture model, in terms of slip and rise time distribution (upper and bottom panel, respectively), obtained by inverting for peak slip velocity and rise time, the 3D dataset in the frequency band 0.01-0.25Hz.

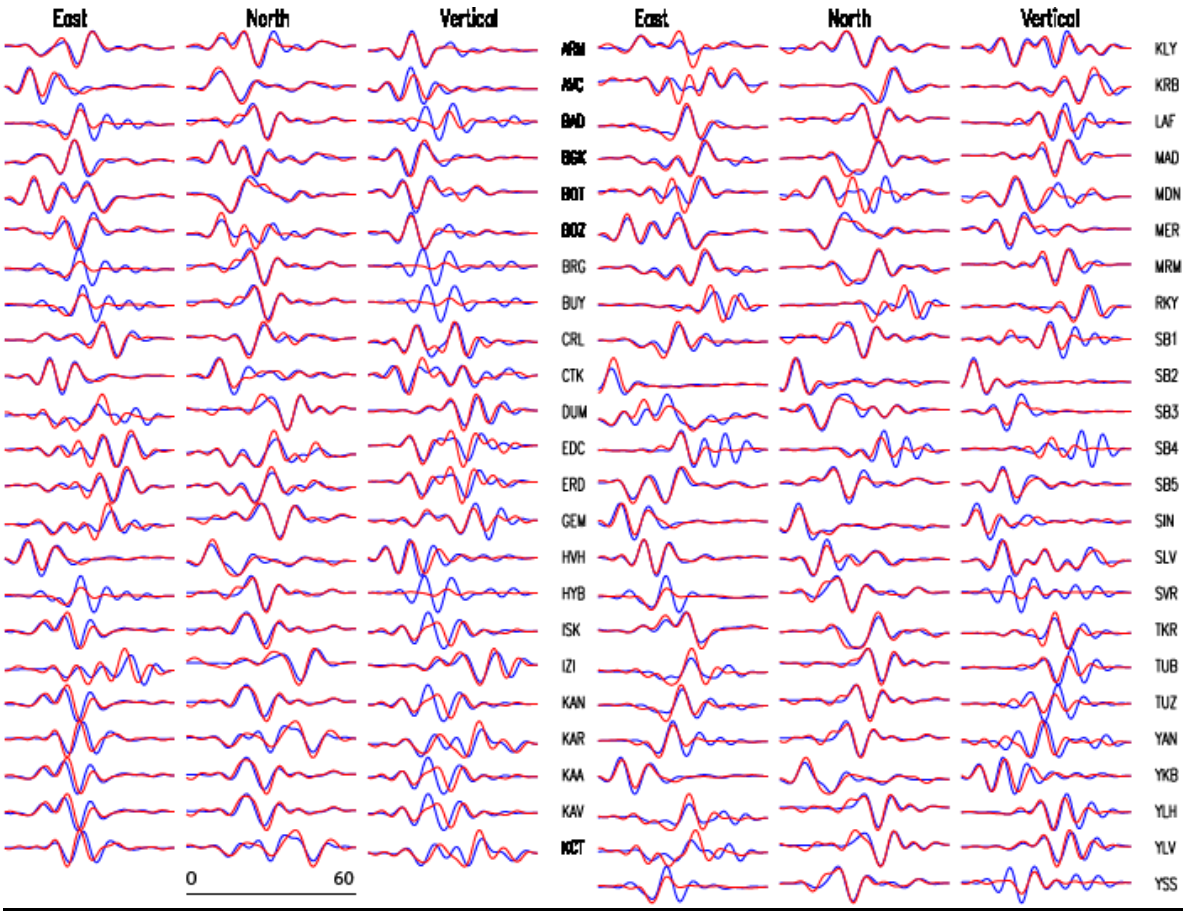

Figure23. Misfit between synthetic ground velocities (blue lines) with those computed from the inverted rupture model displayed in Figure22 (red lines).

Case: 3DonlySlip_0.5Hz

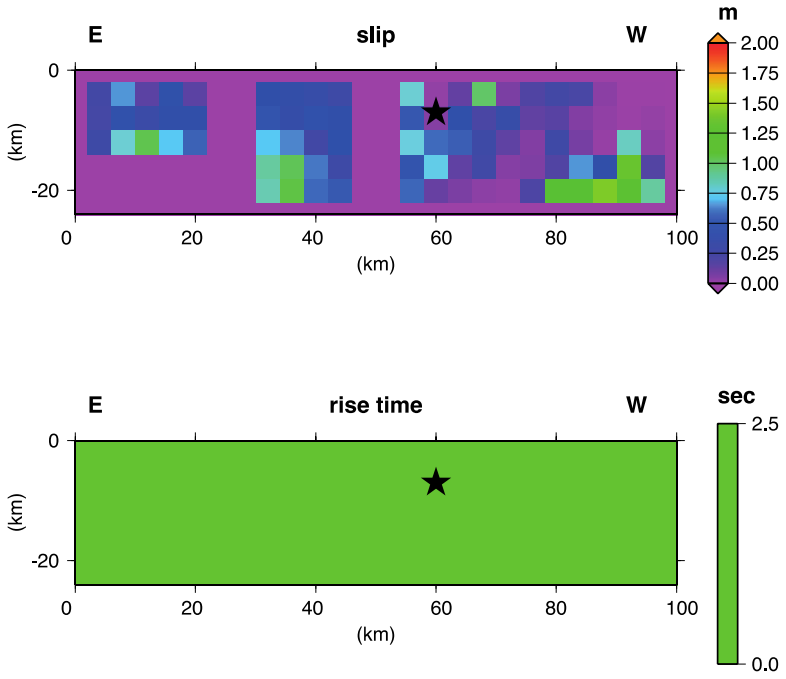

Figure24. Retrieved rupture model, in terms of slip and rise time distribution (upper and bottom panel, respectively), obtained by inverting for peak slip velocity, the 3D dataset in the frequency band 0.01-0.5Hz.

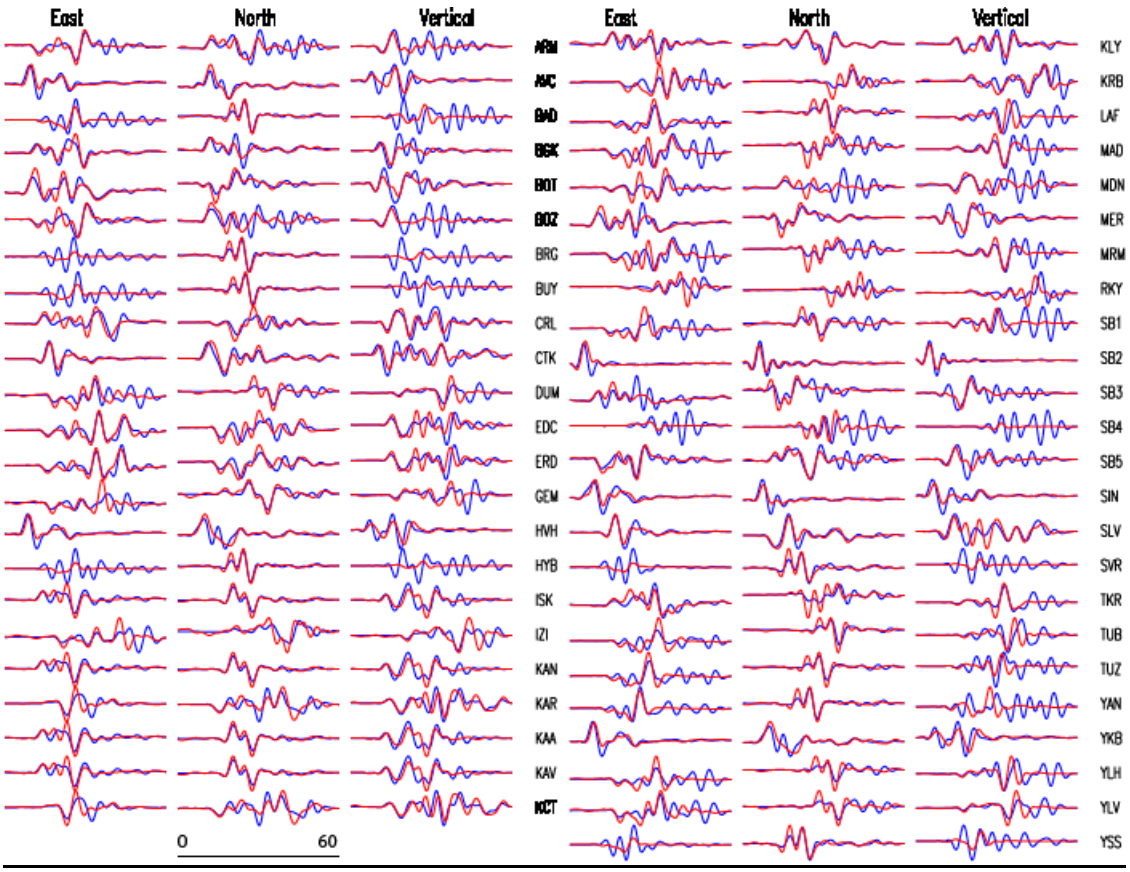

Figure25. Misfit between synthetic ground velocities (blue lines) with those computed from the inverted rupture model displayed in Figure24 (red lines).

Case: 3DSlipRise_0.5Hz

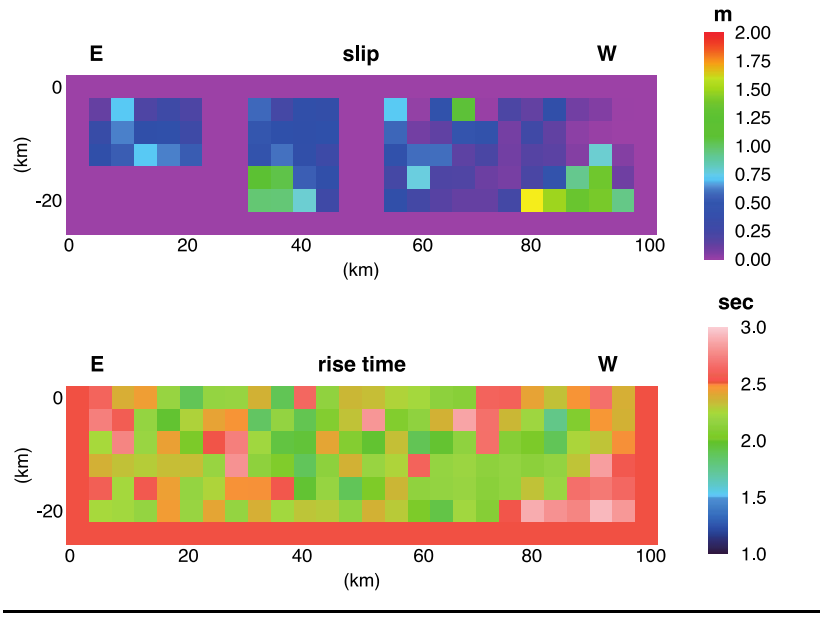

Figure26. Retrieved rupture model, in terms of slip and rise time distribution (upper and bottom panel, respectively), obtained by inverting for peak slip velocity and rise time, the 3D dataset in the frequency band 0.01-0.5Hz.

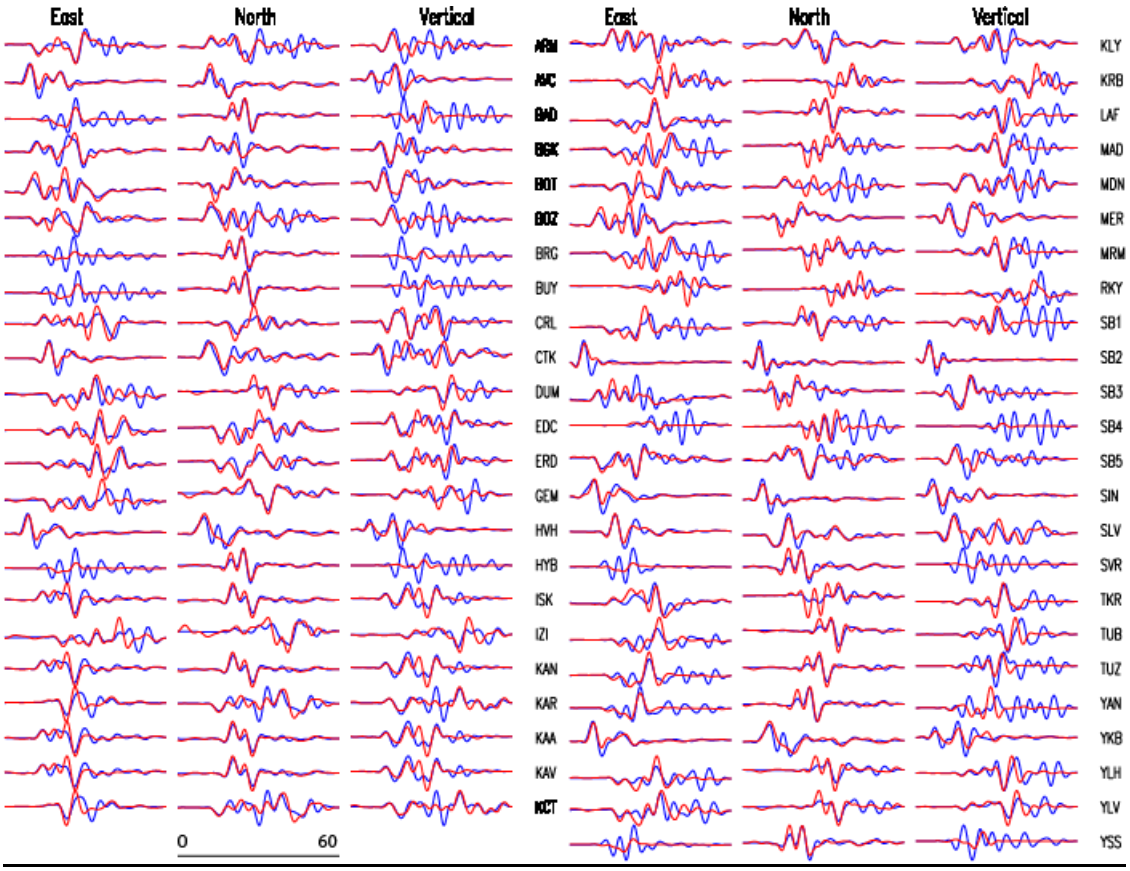

Figure27. Misfit between synthetic ground velocities (blue lines) with those computed from the inverted rupture model displayed in Figure26 (red lines).

The inverted models are similar to the target one (Figure1) ; the positions of the asperities are correctly imaged and the slip values well estimated. In order to quantify and to compare the obtained results, for each performed inversion we show in Table1 the cost function values associated to the waveforms' comparison (second and third column) and the 'SLIP-FIT' comparison (fourth and fifth column). The last 'misfit' is computed by the equation:

$$SLIP\_FIT = \frac{1}{Nsub} \sum_{i=1}^{Nsub} \frac{(slipT - slipR)_i^2}{slipTi^2 + slipRi^2}$$

where $slipT$ and $slipR$ are the target and retrieved slip values and $Nsub$, is the number of sub-faults by which the fault plane has been parameterized. This quantity allows us to quantify the reliability of a retrieved model in respect to the target one and to indicate a preferred performed inversion, in terms of resolution capability. The cost function values' analysis show how the waveform-fit improves with the lower frequency band (see also Figures 13-15-21-23) and it decreases when synthetic data from a 3D earth structure is inverted (Figures 25-27). This is probably due to the difficulty in modelling 3D wave propagation effect. From the 'SLIP-FIT' analysis emerges how the most simple inversion case ('1DonlySlip'), in which we invert just for one parameter (peak slip velocity) and in the lower frequency band (0.01-0.25hz), by using the synthetic dataset generated with a 1D velocity profile, is able to yield a well resolved slip model.

Table1. Cost function values

	WAVEFORM-FIT		SLIP-FIT	
	0.01-0.5Hz	0.01-0.25Hz	0.01-0.5 Hz	0.01-0.25Hz
1DonlySlip	0.33	0.052	0.67	0.59
1DSlipRise	0.31	0.048	0.66	0.60
3DonlySlip	0.45	0.16	0.66	0.61
3DSlipRise	0.44	0.14	0.67	0.61

3. Conclusions

The obtained results show how the proposed inversion techniques guarantee a reliable and accurate reconstruction of earthquake source rupture process on finite fault, in the Marmara tectonic and observational setting configuration. The proposed analysis represents a useful tool to assess the performance of a finite-fault inversion code, by taking into account the actual or future planned stations configuration (strong motion, cGPS, GPS, BB) in the Marmara Sea and earthquake scenarios.

References

Aochi, H., T. Ulrich, A. Ducellier, F. Dupros, D. Michea, Finite difference simulations of seismic wave propagation for unerstanding earthquake physics and predicting ground motions: Advances and challenges, J. Phys: Conf. Ser., 454, 012010, doi: 10.1088/1742-6596/454/1/012010, 2013.

Aochi, H., and T. Ulrich (2014). Dynamic rupture and ground motion simulations in the Sea of Marmara, 2nd European Conference of Earthquake Engineering and Seismology (ECEES), Istabul, Turkey, 24–29 August 2014.

Aochi, H. and T. Ulrich, A probable earthquake scenario near Istanbul determined from dynamic simulations, Bull. Seism. Soc. Am. , 105, doi:10.1785/0120140283, 2015.

Bayrakci, G., M. Laigle, A. Bécel, A. Hirn, T. Taymaz, S. Yolsal-Cevikbilen an SEISMARMARA team, 3-D sediment-basement tomography of the Northern Marmara trough by a dense OBS network at the nodes of a grid of controlled source profiles along the North Anatolian fault, Geophys. J. Int., 194, 1335-1357, 2013.

Cirella A., Piatanesi A., Tinti E. Chini M. and M. Cocco (2012), "Complexity of the rupture process during the 2009 L'Aquila, Italy, earthquake", *Geophysical Journal International.***190**, 607-621, doi:10.1111/j.1365-246X.2012.05505.x

Ji, C., D. J. Wald, and D. V. Helmberger (2002), Source description of the 1999 Hector Mine, California, earthquake, Part I: Wavelet domain inversion theory and resolution analysis, *Bull. Seismol. Soc. Am.*, 92 (4), 1192-1207.

Piatanesi A., A. Cirella, P. Spudich and M. Cocco (2007), "A global search inversion for earthquake rupture history: Application to the 2000 western Tottori, Japan earthquake", *J. Geophys. Res.*, *112*(B7), B07314, doi:10.1029/2006JB004821

Spudich, P. and L. Xu (2003), Software for calculating earthquake ground motions from finite faults in vertically varying media, in *International Handbook of Earthquake and Engineering Seismology*, Academic Press.

Tinti, E., E. Fukuyama, A. Piatanesi and M. Cocco (2005a), A kinematic source time function compatible with earthquake dynamics, *Bull. Seismol. Soc. Am*., 95(4), 1211-1223, doi:10.1785/0120040177.

Zhang, Y., Wang, R., Zschau, J., Chen, Y. T., Parolai, S., & Dahm T., 2014. Automatic imaging of earthquake rupture processes by iterative deconvolution and stacking of high-rate GPS and strong motion seismograms, *J. Geophys. Res.*, **119**, 5633–5650, doi:10.1002/2013JB010469.

Wang, R., 1999, A simple orthonormalization method for stable and efficient computation of Green's functions, *Bull. Seismol. Soc. Am.,* **89**(3), 733–7410.